International Research Journal of Engineering and Technology (IRJET) e-ISSN: 2395-0056
Volume: 09 Issue: 06 | June 2022 www.irjet.net p-ISSN: 2395-0072

Performance of Armor Steel Gas Metal Arc Welded Joints

M.A. Morsy [1], Sabry.M. Abdel Aziz [2, *], Khaled Abdelwahed [3], Sabreen A. Abdelwahab [4]

[1] Professor and Head of Welding and NDT Department, CMRDI, Cairo, Egypt.
*[2, *] Ph.D. Student, Department of Production Technology, Faculty of Technology and Education, Helwan University, Cairo, Egypt.*
[3] Assistant Professor, Department of Automotive and Tractors Technology, Faculty of Technology and Education, Helwan University, Cairo, Egypt.
[4] Associate Professor, Department of Production Technology, Faculty of Technology and Education, Helwan University, Cairo, Egypt.

Abstract - *The existence of tempered martensite in microstructure for armor steel makes the material sensitive to heat input and any thermal process. Thus, welding of this steel can negatively affect the welded joint's properties. In MAG welding process using AWS A5.18 ER70S-6 filler wire, both single V and single bevel joints passed the required tensile strength by the military standard. Moreover, with MIG welding process using AWS A5.9 ER307 filler wire, both joints passed the required tensile strength by the military standard.*

Dilution was observed in single V welded joints using both carbon steel and austenitic stainless-steel filler metal. The dilution percentage increased in single bevel welded joints more that the obtained in single V joints using both carbon steel and austenitic stainless steel. An increase in cooling rate resulted in a significant increase in joint strength and retainment of base metal hardness value at a shorter distance from the centerline of weld metal (lower than 14 mm). A softening region at the HAZ is formed due to the over-tempering of the martensitic structure with a reduction in hardness values. This softening zone is much reduced in width with the increase in its hardness values with the application of cooling and reduction of heat input.

Both single V-joint and single bevel joint passed the required absorbed energy in Charpy V notch impact at - 40 °C tests whether using carbon steel and austenitic stainless-steel filler wire.

Results show that the corrosion rates of welded joints are lower than the base metal. It is worthy to mention that the single bevel welded joints give much lower corrosion rates than the base metal and the single bevel welded joints performed using austenitic stainless-steel filler wire compared to single bevel welded joint performed using carbon steel filler wire. The results were discussed on the basis of the mechanical properties and metallurgical properties of the welded joints.

Key Words: Gas metal arc welding (GMAW) process; armor steel welded joints; carbon steel filler metal; austenitic stainless-steel filler metal; welding parameters; metallurgical properties; mechanical properties, corrosion behaviour test

1.INTRODUCTION

In recent years, there are accelerated efforts to deliver armor technologies that can defeat armor-piercing projectiles. The selection of steel alloys continues to be competitive for numerous ballistic and structural applications where the use of ultrahigh strength steel plates resulted in the decrease in the weight of armor structure with good ballistic properties [1].

The Armox 500 T belongs to the category of the fine-grained, increased-strength steels, sometimes-called ballistic steels are classified in the AWS standards and in military standards [2]. A combination of the standards is used to classify and identify the metal and methods to process it, which are manufactured by the quenching and tempering process [3].

Therefore, these steels have high strength, hardness, and good toughness where acquired these materials strength up to 1000 MPa. Most of the higher processed materials that exceed this range are identified in the military standard MIL-St A46100 [4]. The issue with the armor steel is that it reaches very high hardness (around 500 HV) and tensile strength (around 1650 MPa) using complicated processing called thermomechanical controlled processing (TMCP) at high temperatures, including quenched and tempering. This process resulted in the fine grains martensitic structure with ultrahigh strength properties. Considering that this makes the steel sensitive to any thermal processing including cutting and welding processes [5,6].

Armor steels are used in military applications and counters for banks, doors, and vehicles for safely people and money transport, and tanks body shielding, and police vehicles [7].

An armor has three main roles in order to ensure the protection and integrity of the combat vehicle and its occupants. These three roles are often described as absorption of the penetrator's energy and/or transfer of energy to the supporting structure; rebounding or charging of direction of the penetrator away from the vehicle, and deformation of the penetrator [8].

The welding characteristics of armor steel depend on the gap between plates, types of base materials, filler wire type is used, welding voltage, welding current, wire feed rate, shielding gas, and the skill of the operator. Therefore, these parameters should be controlled in order to achieve the desired weld quality [9,10].

Nominal composition %										
Elements	C max	Si max	Mn max	P max	S max	Cr max	Ni max	Mo max	B max	Fe
Standard	0.32	0.4	1.2	0.010	0.003	1.0	1.8	0.7	0.005	Bal

Armox 500 T armor steel [11] has good weldability according to the chemical composition because its carbon equivalent is relatively low (0.56) [12].

$$CE = C + Mn/6 + (Cr + Mo + V)/5 + (Ni + Cu)/15 \ [\%] \quad (1)$$

Requirements of quality for the welding of MIL-A-46100 steel are given by MIL-STD 1185 and SD-X12140 standards. The requirements are divided into three categories: (i) mechanical properties, (ii) weld soundness, and (iii) in-service performance [13].

Military standards demonstrate that the ultimate tensile strength of welded joints should exceed 750 MPa to be succeeded using carbon steel filler metal. However, they should exceed a minimum ultimate tensile strength of 550 MPa using austenitic stainless-steel filler metal. The retainment of base metal hardness value must be achieved at a distance of 16 mm measured from the centreline of the weld bead. The Charpy V notch impact test results of both weld metal and heat-affected zone are also important [6,13].

The aim of the research work is to investigate the weldability of Armox 500 T armor steel using the GMAW process. Two types of filler metals will be applied and also two types of joint configuration will be used. The effect of heat input and cooling rate will be studied. The results will be discussed on the basis of mechanical, metallurgical and corrosion properties of the welded joints.

2. METHODS AND EXPERIMENTAL PROCEDURE

This section describes the used materials and experimental and testing methods.

2.1. Materials

The base metal was ARMOX 500 T which is a commercial name for armor sheet metals with a dimension of 200*155*10 mm. The heat treatment includes austenitizing at 900 ºC then water quenching and followed by tempering at 200 ºC [14]. The obtained base metal has high hardness and strength with acceptable toughness. The chemical composition and mechanical properties from the SSAB company specification of base metal as presented in Tables 1 and 2.

Table -1: Chemical compositions of the Armox 500 T steel plate, (SSAB company specification), wt. %.

Table -2: Typical mechanical properties of the Armox 500 T steel plate, (SSAB company specification).

Hardness (HBW)	Yield strength (MPa)	Tensile strength (MPa)	Elongation (%)	Charpy V notch impact test specimen (10*10 mm) at - 40ºC
480-540	1250	1450-1750	8	32 (J)

2.2. Welding joints fabrication and thermocouple location

In this investigation, two different weld groove shapes namely single V and single bevel grooves were fabricated using machine CNC high-speed wire cut EDM (model FW 2U series - Switzerland). An impermeable hole with a diameter of 1 mm was carried out in the centreline of specimens at a distance of 2.89 mm from the root edge of the groove as shown in Fig.1. With a depth of 3 mm from the bottom of the sample, using CNC electrical discharge forming machine (model DM 450 series - China). A K-type thermocouple is inserted in the hole to measure the temperature change in the heat-affected zone (HAZ).

2.3. Welding process and shielding gas

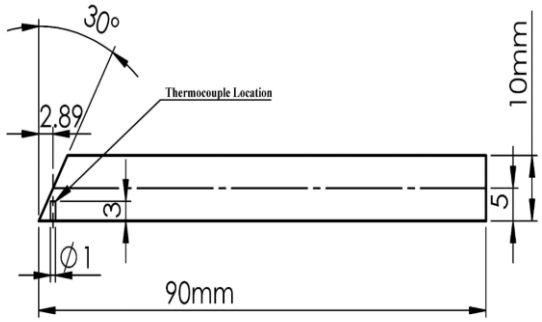

Fig -1: Schematic drawing of edge preparation showing thermocouple location.

In this research work, the gas metal arc welding GMAW is applied. A welding machine type (Fronius VARIO STAR 457-2) is used. The welding parameters and conditions are listed in Tables 3, 4, and Fig.2. The welder tries to apply the lowest level filler wires of welding current in order to reduce the deterioration of HAZ microstructure as a result of softening [6,15,16]. The gas used with ER 70S-6 carbon steel filler metal (100% CO2) with a flow rate of 12 l/min in MAG. However, Argon gas 100 % is used in the case with ER 307 filler metal with a flow rate of 14 l/min in MIG. The diameter of AWS A5.18 ER70S-6 wire is 0.8 mm, however the diameter of AWS A5.9 ER307 wire is 1.2 mm. Using austenitic filler metal is an advantage to decrease the susceptibility to cold cracking [6,16].

* The heat input is determined using equation (2)

$$Hi = \mu \frac{V\,I\,60}{S\,1000} \quad \text{(kJ/mm)} \qquad (2)$$

Hi: Heat input (kJ/mm)
V: Arc voltage (Volts)
I: Current (Amperage)
μ: Thermal efficiency (GMAW = 0.8)
S: Travel speed (mm/min)

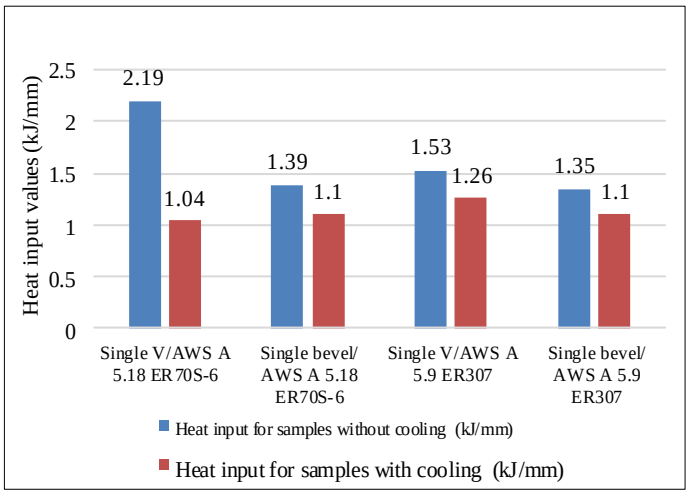

Fig-2: Heat input values of all specimens.

Table -3: Welding procedure parameters.

Samples	Number of passes	Welding current (A)	Arc voltage (V)	Wire feed (m/min)	Travel speed (mm/min)	Heat input (kJ/mm) *
Single V / AWS A 5.18 ER 70S-6 without cooling	5	195	27.5	7.5	117.23	2.19
Single bevel/ AWS A 5.18 ER70S-6 without cooling	5	195	27.5	7.5	183.93	1.39
Single V/ AWS A 5.9 ER 307 without cooling	4	219	24.5	7.7	167.59	1.53
Single bevel/ AWS A 5.9 ER 307 without cooling	4	219	24.5	7.7	190.18	1.35
Single V/ AWS A 5.18 ER 70S-6 with cooling	4	160	25	7.5	183.07	1.04
Single bevel/ AWS A 5.18 ER70S-6 with cooling	3	160	25	7.5	170.72	1.1
Single V/ AWS A 5.9 ER 307 with cooling	3	220	24.5	7.7	200.20	1.26
Single bevel/ AWS A 5.9 ER 307 with cooling	3	220	24.5	7.7	211.21	1.1

Table -4: Welding procedure conditions.

Base metals	ARMOX 500 T			
Thickness of plate	10 mm			
Welding process type	GMAW			
Welding machine type	Fronius (VARIOSTAR 457-2)			
Filler metal type	AWS A5.18 ER 70S-6	AWS A 5.9 ER 307	AWS A5.18 ER 70S-6	AWS A 5.9 ER 307
Joint type and angle	Single V (60º) and Single bevel (30º)			
Filler wire diameter (mm)	0.8	1.2	0.8	1.2
Gas (%)	100% CO2	100% Argon	100% CO2	100% Argon
Gas flow rate l/min	12	14	12	14
Welding methods	Continuous		Not continuous	
Cooling method	Without cooling (left at ambient temperature after completion of the whole welding)		With using compressed air (6 bar) in the cooling after each pass up to 100ºC	

2.4. Filler metal Types

Two filler metals are used with the GMAW process one is a carbon steel AWS A 5.18 ER 70S-6 and the other is an austenitic type AWS A 5.9 ER 307. The selection was based on the results obtained in previous literature by [6,15,16,17] and filler metal manufacturers' specifications [18,19,20] and requirements for the welding of armor steel according to MIL-STD 1185 standards [21]. Using austenitic filler metal is an advantage to decrease the susceptibility to cold cracking [15, 17]. The welder tries to apply the lowest level filler wire welding current in order to reduce the deterioration of HAZ microstructure as a result of softening [6,15,16,22,23].

2.5. Metallurgical properties of the joints

An optical emission spectrometry equipment is used to determine the chemical compositions of base metal and weld metals. The cross-sections were prepared for metallurgical observations. This includes grinding by sandpapers from 100 to 1000 mesh and finally polished using alumina paste. Etching using a 2 % Nital solution was used to reveal the martensitic structure. However, 10 % oxalic acid was used to reveal the austenitic structure. Microstructure characteristics of weld metal (WM) at various locations, base metal (BM), and heat-affected zone (HAZ) regions were observed by an optical microscope (OLYMPUS MODEL PMG3 - F3). A stereoscope is used to show the macrostructure of welded joints. The dilution percentage was calculated using the equation (3) illustrated in Fig.3. [24].

$$\text{Dilution (\%)} = A+B/A+B+C *100 \quad (3)$$

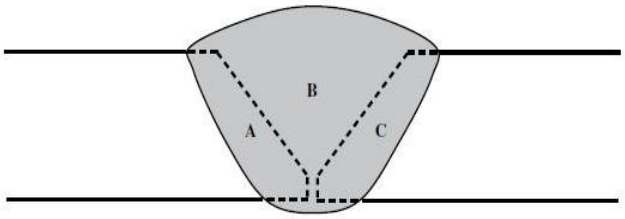

Fig -3: Calculation of percent dilution

2.6. Mechanical properties of the joints

Hardness distributions have been carried out by using the Vickers hardness testing machine model (DVK-2 Tokyo Japan) was employed with a 20 kg load for 70 seconds to measure the hardness distribution at the welded joints. The hardness profile through weld metal, HAZ, and the base metal will be determined with a pitch of measurement position of 1 mm. The test has been carried out according to ASTM standards [25]. Transverse tensile tests have been carried out using a tensile machine model (Universal Testing Machine WDW-300 China). The test has been carried out according to ASTM A370-12 [26], using two specimens. Charpy V notch impact test was done using a Charpy V notch impact testing machine using a low-temperature chamber at -40 °C and also at room temperature. Charpy impact tests in the weld metal and HAZ were performed according to ASTM E23 - 12 c standard [27]. Five readings were taken in each location.

2.7. Corrosion behaviour test

The corrosion behaviour of base metal and welded joints was investigated using electrochemical corrosion testing apparatus (Auto lab NOVA 2.1.5) in 3.5wt% NaCl solution at room temperature [28]. Samples were corrosion tested using potentiodynamic polarization and electrochemical impedance (EIS) techniques. Samples were polished up to 1200-grit finish, ultrasonically cleaned and rinsed with ethanol, and finally dried. A conventional three-electrode cell in a single compartment-cylindrical glass cell was used with a Pt counter electrode. All the potentials were recorded with respect to a saturated calomel electrode (SCE) reference electrode at 25oC. Sodium chloride medium was prepared from analytical grade chemicals and bi-distilled water. The potential was scanned starting from -0.3 V below Ecorr in the positive direction (~ 1 V above Ecorr). Corrosion parameters; corrosion potential (Ecorr), Corrosion current (Icorr), and corrosion rate (CR) were deduced from the polarization curves using AutoLab software as shown in Fig.4.

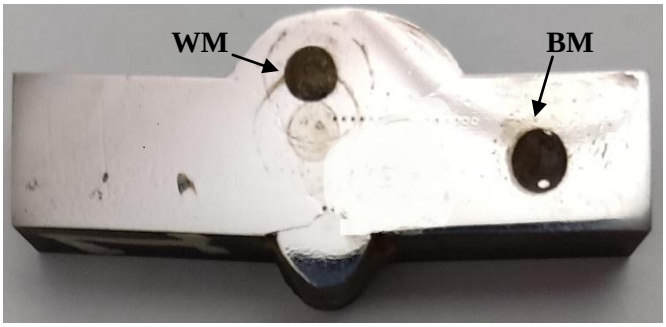

Fig -4: Corrosion shape on the sample in BM, and WM region

3. RESULTS AND DISCUSSION

3.1. Chemical compositions of base metal

The chemical analysis of base metal from SSAB company specification and actual analysis for base metal is presented in Table 5. The mechanical properties are shown in Table 6.

3.2. Chemical compositions of weld metal

The chemical composition of all weld metals is shown in Table 7.

Table -5: Chemical compositions of the Armox 500 T steel plate, wt. %

Elements	C	Si	Mn	P	S	Cr	Ni	Mo	B	CE	Fe
Company specification	0.32 max	0.4 max	1.2 max	0.010 max	0.003 max	1.0 max	1.8 max	0.7 max	0.005 max	0.67 max	Bal
Actual analysis	0.154	0.2	0.88	0.009	0.003	0.5	0.89	0.36	0.001	0.56	Bal

Table -6: The mechanical properties of the Armox 500 T steel plate.

Hardness (HV)	Yield strength (MPa)	Tensile strength (MPa)	Elongation (%)	Charpy V notch impact test specimen (10*10*55 mm) at - 40 ºC
450	1250	1650	8.9	34 (J)

Table -7: The chemical composition of all weld metals, wt. %.

Elements	C		Si	Mn	P	S	Cr	Ni	Mo	V	Fe
AWS A 5.9 ER 307	0.09		0.9	7	0.001	0.002	19	8.5	0.13	0.03	Bal
AWS A 5.18 ER 70S-6	0.07		0.8	1.45	0.002	0.003	0.025	0.05	0.002	0.012	Bal

3.3. Thermal cycle analysis

The cooling rate is determined using two temperature ranges. One between 800 °C to 500 °C and the other range between 600 °C and 200 °C [29].

Figure 5 shows the cooling rate of welded samples without using compressed air after completion of welding. The cooling time (Δt 8/5) of the first pass is 30 seconds, the cooling rate (Δt 8/5) is 10 °C/sec. The cooling rate (Δt 8/5) of the second, the third, and the fourth passes is 11 °C/sec. The cooling time (Δt 6/2) of the first pass is 230 seconds and the mean cooling rate (Δt 6/2) is 1.73 °C/sec. The cooling rate (Δt 6/2) of the second, the third, and the fourth passes is 1.63 °C/sec.

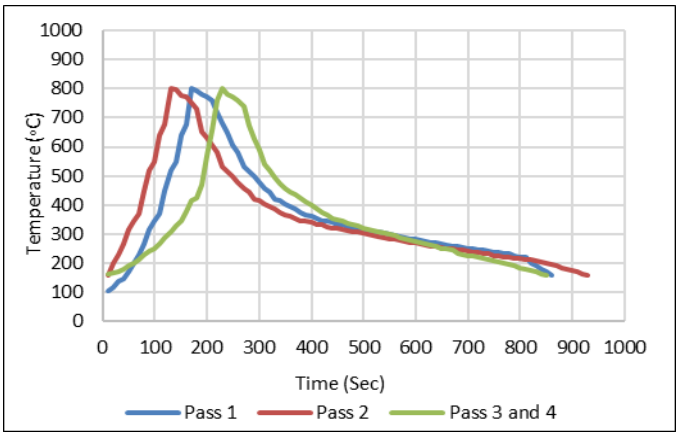

Fig -5: Temperature cycle for single V using AWS A 5.9 ER307 without cooling.

Figure 6 shows the cooling rate at the HAZ with the application of compressed air immediately after completion of welding. The cooling time (Δt 6/2) of the first pass is 110 seconds, the second pass is 110 seconds, the third pass is 150 seconds, and the fourth pass is 120 seconds. The cooling rate (Δt 6/2) of the first pass is 3.64 °C/sec, the cooling rate (Δt 6/2) of the second pass is 3.64 °C/sec, the cooling rate (Δt 6/2) of the third pass is 2.66 °C/sec, and the cooling rate (Δt 6/2) of the fourth pass is 3.33 °C/sec.

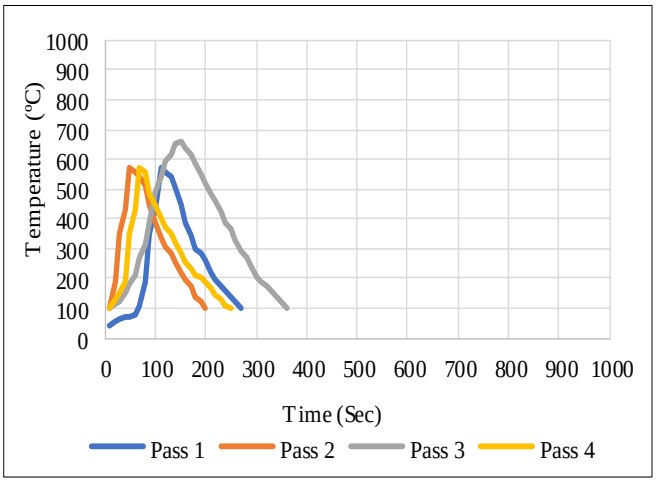

Fig -6: Temperature cycle for single V / ER 70S-6/ MAG with cooling.

Figure 7 shows the cooling rate at the HAZ with the application of compressed air immediately after completion of welding. The cooling time (Δt 6/2) of the first pass is 110 seconds, the second pass is 160 seconds, the third pass is 170 seconds. The cooling rate (Δt 6/2) of the first pass is 3.64 °C/sec, the cooling rate (Δt 6/2) of the second pass is 2.5 °C/sec, and the cooling rate (Δt 6/2) of the third pass is 2.35 °C/sec.

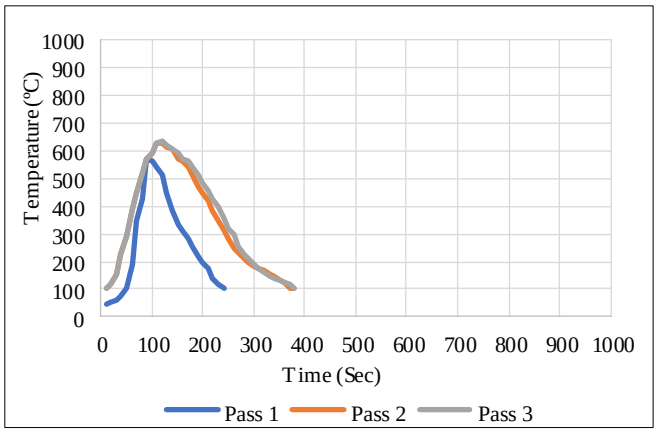

Fig -7: Temperature cycle for single bevel / ER 70S-6/ MAG with cooling.

Figure 8 shows the cooling rate at the HAZ with the application of compressed air immediately after completion of welding. The cooling time (Δt 8/5) of the first pass is 70 seconds, the cooling rate (Δt 8/5) is 4.29 °C/sec. The second pass is 70 seconds, the cooling rate (Δt 8/5) is 4.29 °C/sec. And the cooling time (Δt 6/2) of the first pass is 160 seconds, the cooling rate (Δt 6/2) is 2.5 °C/sec. The cooling rate (Δt 6/2) of the second, and the third passes is 2.5 °C/sec, and 3.64 °C/sec, respectively.

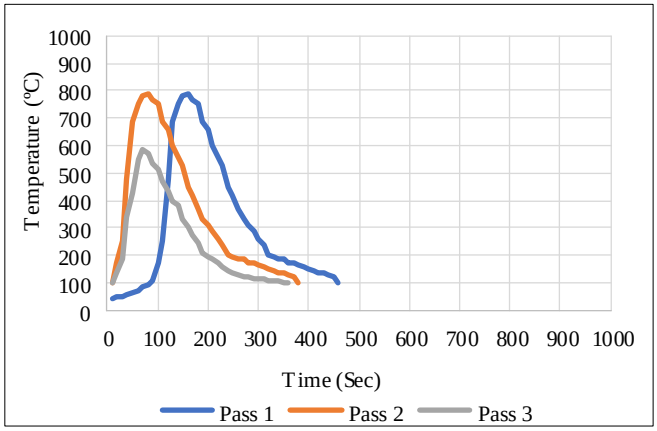

Fig -8: Temperature cycle for single V / ER 307/ MIG with cooling.

Figure 9 shows the cooling rate at the HAZ with the application of compressed air immediately after completion of welding. The cooling time (Δt 6/2) of the first pass is 150 seconds, the second pass is 120 seconds, the third pass is 120 seconds. The cooling rate (Δt 6/2) of the first pass is 2.66 °C/sec, the cooling rate (Δt 6/2) of the second pass is 3.33 °C/sec, and the cooling rate (Δt 6/2) of the third pass is 3.33 °C/sec.

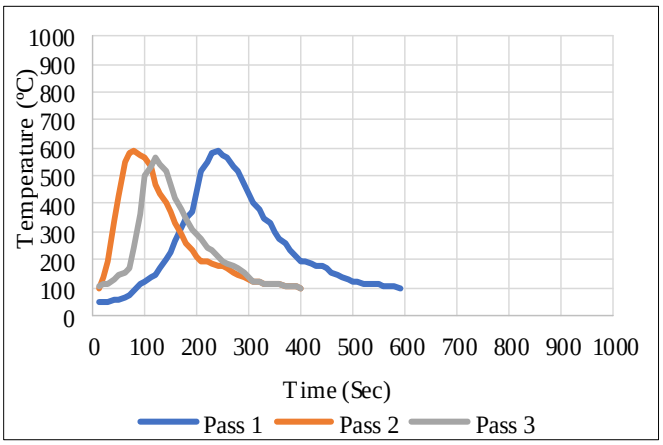

Fig -9: Temperature cycle for single bevel / ER 307/ MIG with cooling.

3.4. Macrostructures of the welded joints

The macrostructures of all the welded joints are shown in Fig. 10. As can be seen from the mentioned Figures, all of the samples (except for sample c) have a significant reinforcement due to the final two layers this occurs as a consequence of the reduction amperage and increases in welding speed. The welded joints are all homogenous without the occurrence of pores or inclusions or cracks. Penetration of all weld passes is sufficient and no lack of fusion was noticed.

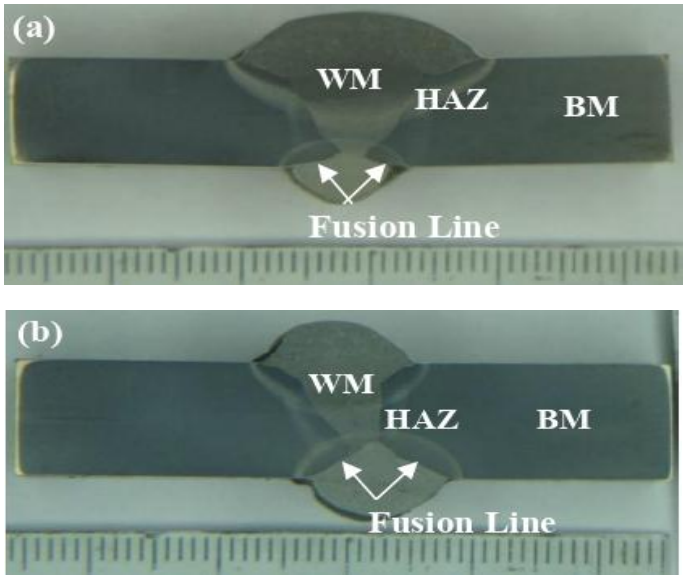

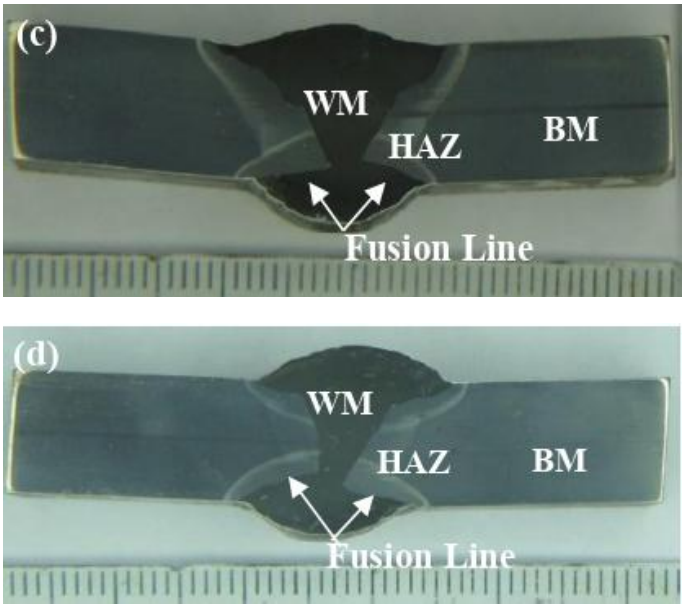

Fig -10: Macrographic of welded samples a) single V/ ER70S-6/ MAG with cooling b) single bevel/ ER70S-6/ MAG with cooling c) single V/ ER307/ MIG with cooling d) single bevel/ ER307/ MIG with cooling.

3.5. Microstructure observations

Figure 11.a shows the microstructure of the base metal. It is tempered martensite with retained austenite. Figure 11.b shows the SEM observation of base metal which is a lath of martensite structure that occurs due to the low tempering temperature of the heat-treatment process.

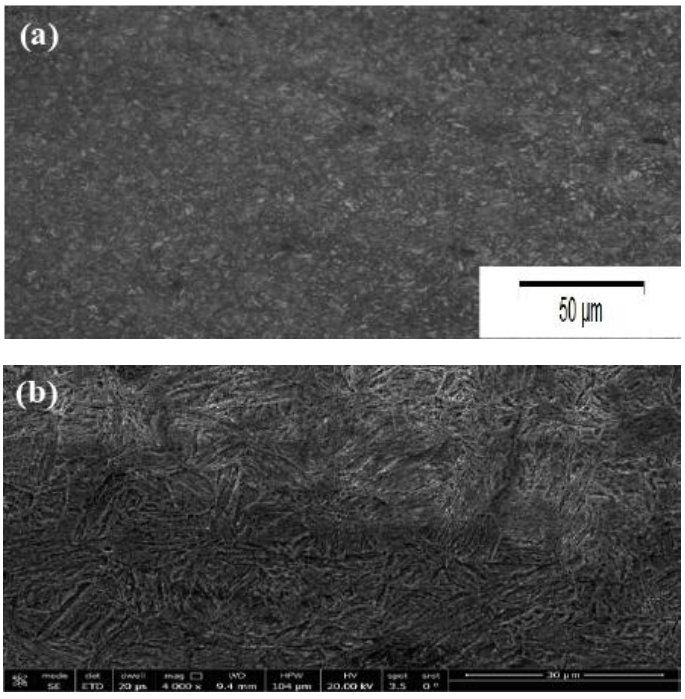

Fig -11: The microstructure of the base metal (ARMOX 500 T) armor steel a) optical microscope b) SEM observation.

Figure 12.a shows the microstructure of weld metal WM using carbon steel wire for a single V-joint groove, it is a columnar structure composed of polygonal ferrite and acicular ferrite. Figure. 12.b shows the microstructure of the weld metal and heat-affected zone. Heat-affected zone shows the over-tempering of martensitic structure. Figure. 12.c shows the microstructure of the over-tempered zone consists of martensitic and over-tempered martensite structures. However, Figure 12.d shows the over-tempered (softening zone) which is exposed to a temperature lower than AC1.

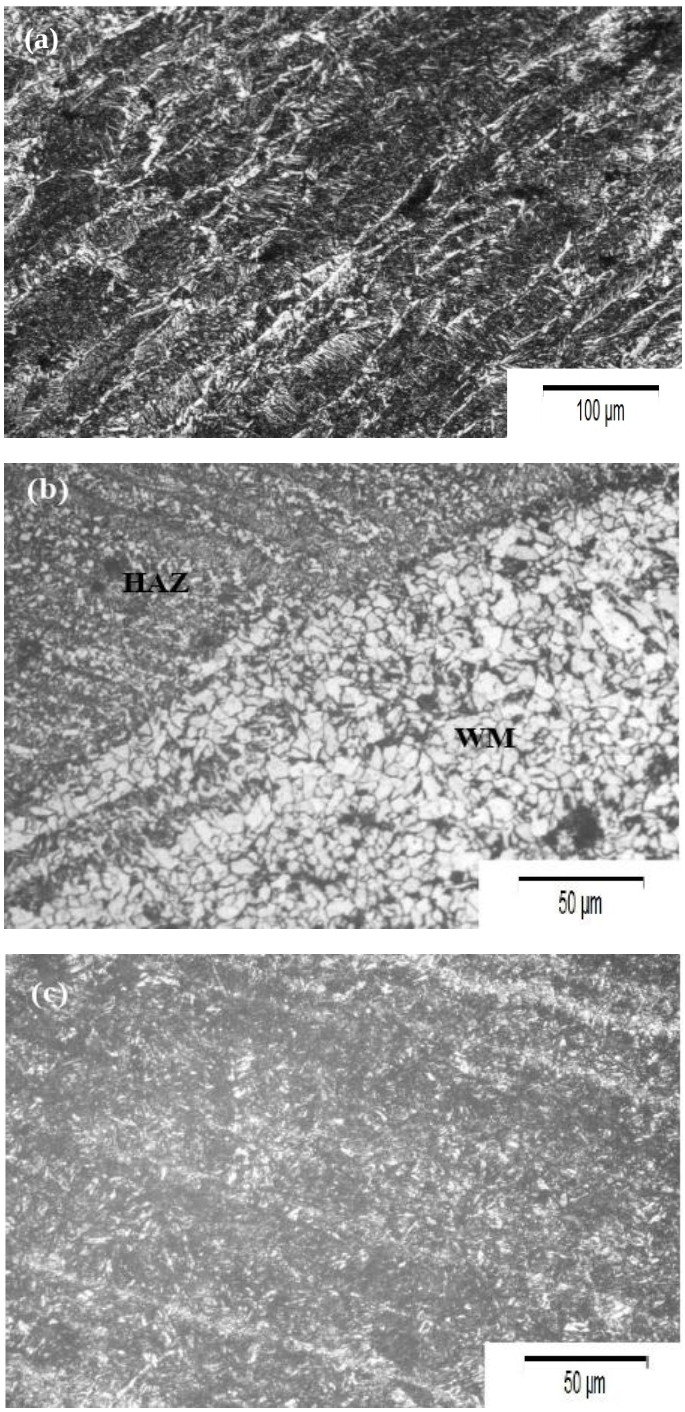

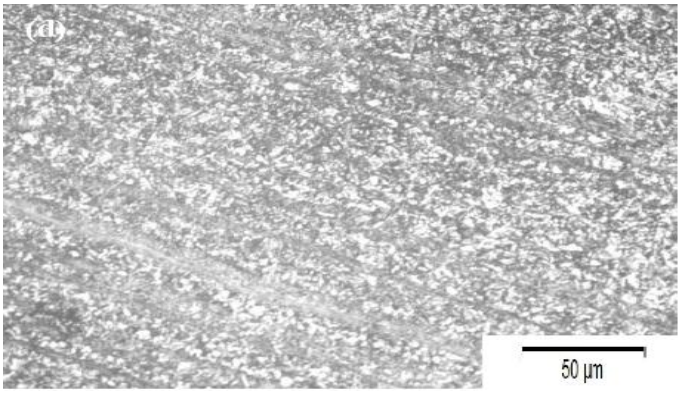

Fig -12: Microstructure of single V welded joint using AWS A 5.18 ER70S-6 filler metal a) weld metal b) weld metal and HAZ c) over-tempered zone composed of martensitic and over-tempered martensite d) over-tempered (softening zone).

Figure. 13.a shows the microstructure of the weld metal region in the joint welded using carbon steel filler wire with single bevel joint groove preparation. It is columnar grain and ferrite and pearlite. Figure. 13.b shows the cellular structure in the weld metal region and this occurs due to the annealing process generated by multiple passes of welding in this region. Figure. 13.c shows the microstructure of heat affected zone (HAZ). It is a martensitic structure region that reaches the austenitic and cooled rapidly to form a martensitic structure. However, Figure. 13.d shows the over-tempering (softening zone) that reaches over than AC1 temperature that case over-tempering and softening of microstructure.

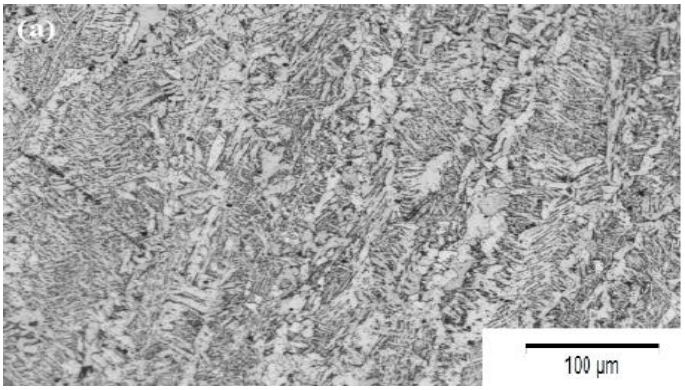

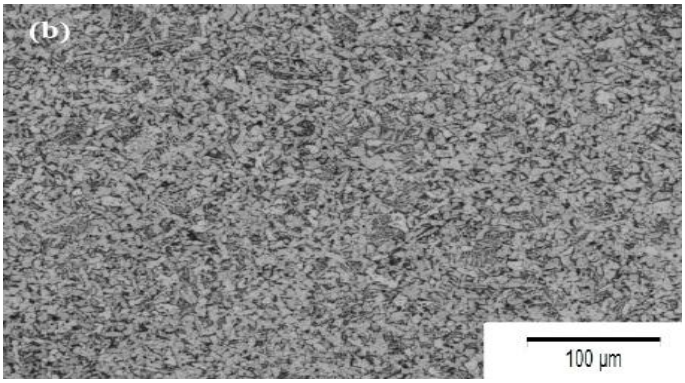

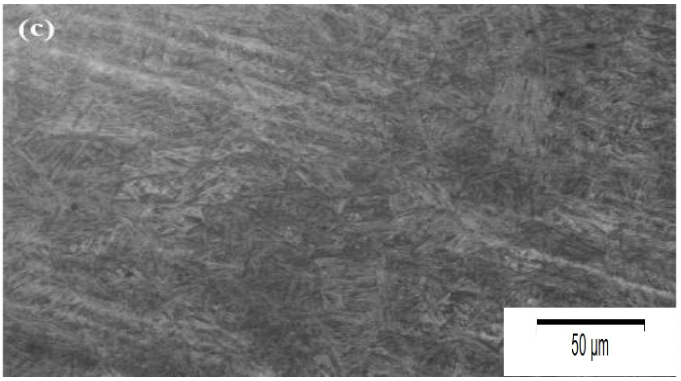

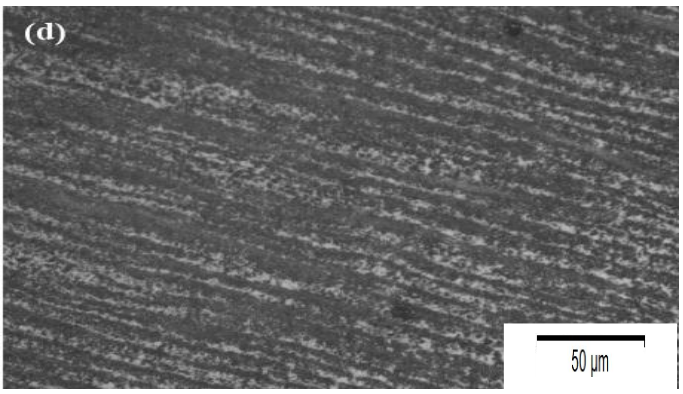

Fig -13: Microstructure of single bevel welded joint using AWS A 5.18 ER70S-6 filler metal a) weld metal b) cellular structure zone in weld metal c) martensitic structure in HAZ zone d) over-tempering (softening zone).

Figure. 14. a and 14.b shows the microstructure of the weld metal using austenitic stainless-steel wire single V- joint groove, it is the austenitic columnar structure. and indicates that the weld cap reflected low dilution at the cap. However, Figure.14. c shows the microstructure of the HAZ for a single bevel-joint groove, it is the grain coarsening martensitic structure, and this indicates that this region reached about to temperature 1250 ºC which caused grain coarsening, Figure.14. d shows the existence of grain refinement martensite structure, and this indicated that this region reached a temperature of about 900 ºC. Figure. 14. e shows the existence of over tempering microstructure in the HAZ zone as indicated by the rise of these regions' temperature to a high value lower than the austenitizing temperature yet over tempering temperature.

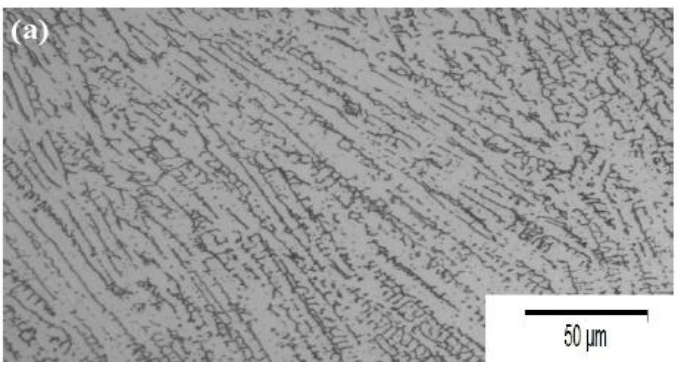

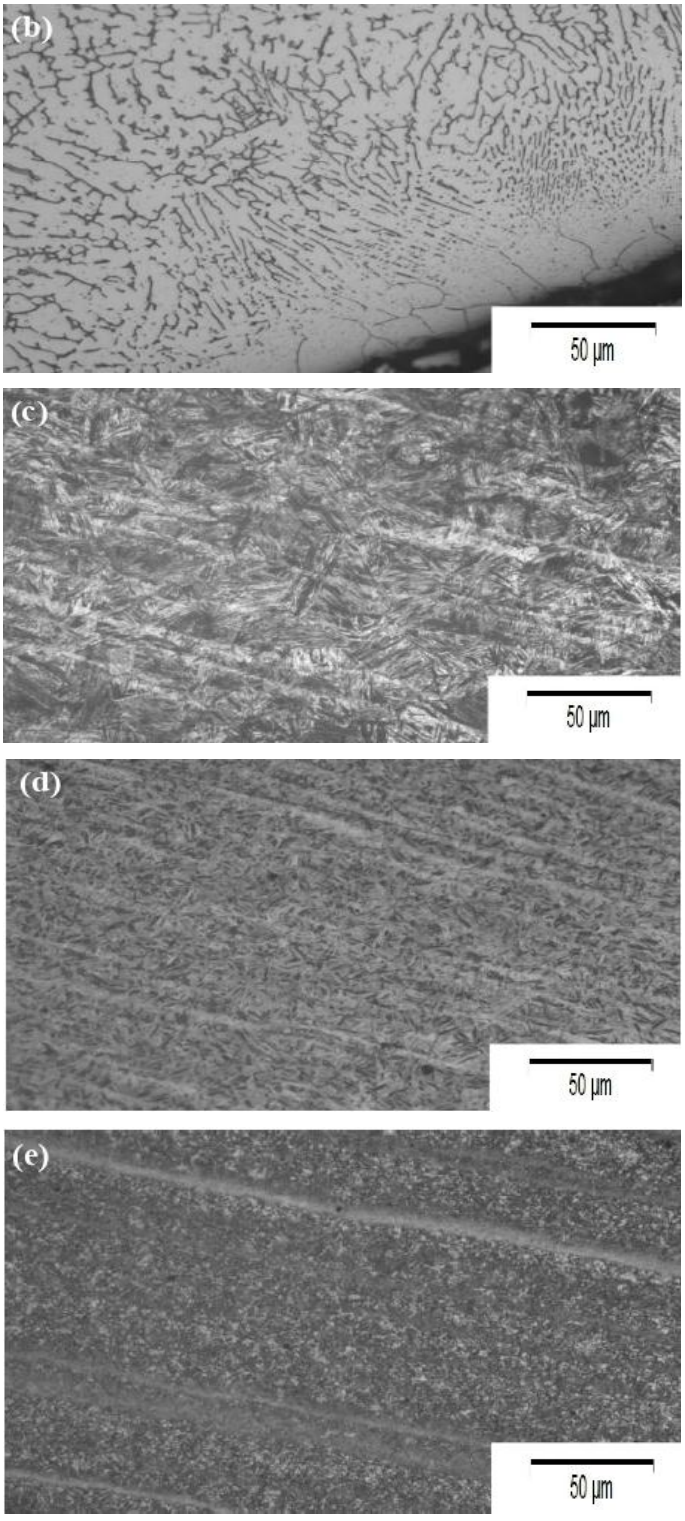

Fig -14: Microstructure of single V welded joint using AWS A 5.9 ER307 filler metal a) and b) weld metal c) the microstructure of HAZ grain coarsening martensitic structure d) grain refinement martensite structure e) over-tempering (softening zone).

Figure. 15. a show the microstructure of the weld metal using austenitic stainless-steel wire single bevel-joint groove, it is the austenitic columnar structure. Figure.15. b shows the martensitic structure at the edge of the joint in the weld metal of the root zone (close to HAZ) and this reflects the high dilution percentage of the weld metal armor steel base metal (see section 3.7). Figure. 15. c shows the microstructure of the HAZ for a single bevel-joint groove, it is the grain coarsening martensitic structure, and this indicates that this region reached about to temperature 1250 ºC which caused grain coarsening, Figure.15. d shows the existence of grain refinement martensite structure, and this indicated that this region reached a temperature of about 900 ºC. Figure. 15.e shows the existence of over tempering zone microstructure (softened zone) and this indicates that these regions were exposed to a temperature that caused over tempering of microstructure.

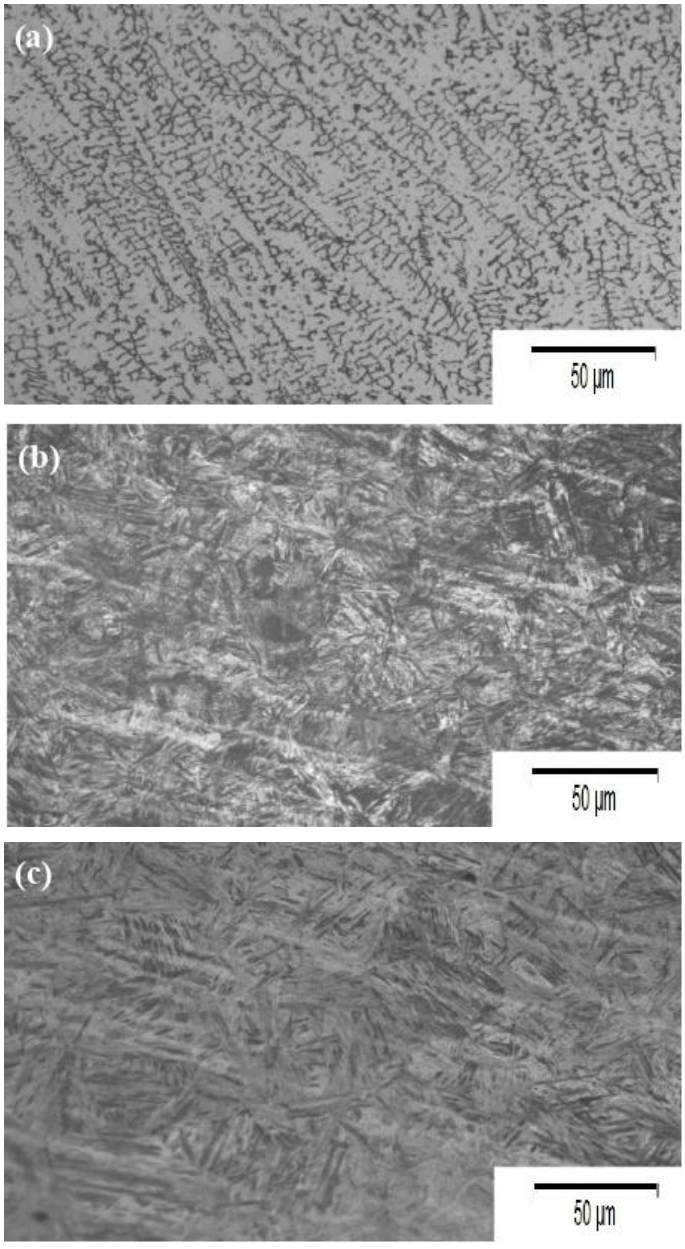

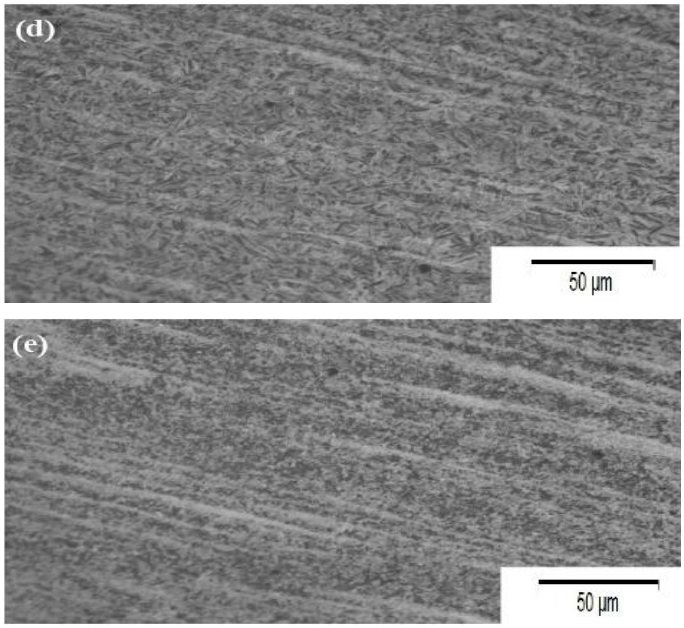

Fig -15: Microstructure of single bevel welded joint using AWS A 5.9 ER307 filler metal a) weld metal b) martensite structure in HAZ zone c) the microstructure of HAZ grain coarsening martensitic structure d) grain refinement martensite structure e) over-tempering (softening zone).

3.6. Hardness distribution

Figure. 16 shows the hardness distribution of the joint welded using AWS A5.18 ER70S-6 filler wire and applying a single V-groove joint. The hardness values abruptly increased from the weld metal in the grain coarsening zone of the HAZ. The hardness then decreases to a lower value than that of the base metal. This could be attributed to the over tempering of this zone. The hardness again increases to reach to near that of the base metal. Application of cooling resulted in the significant retainment of base metal hardness at a distance of 14 mm (455 HV) from the centreline of weld metal. The high weld metal hardness at the root could be attributed to the higher dilution of weld metal from base metal.

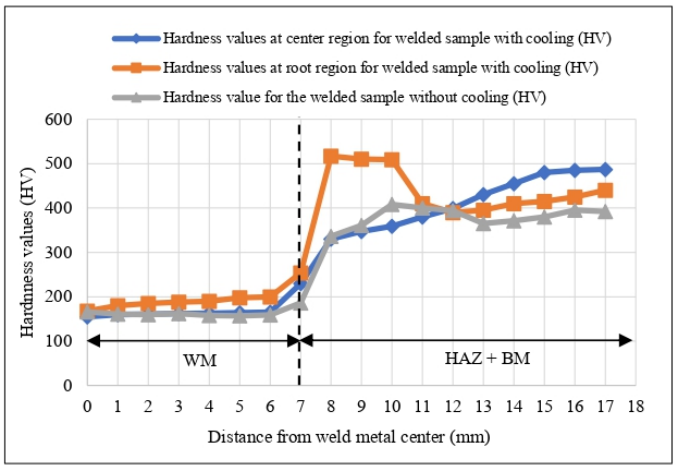

Fig -16: Hardness distribution in the specimen welded using AWS A5.18 ER 70S-6 / MAG and applying single V joint.

Figure. 17 shows the hardness distribution of the joint welded using AWS A5.18 ER70S-6 filler wire and applying a single bevel groove joint. It can be concluded that the application of a single bevel groove with cooling resulted in a retainment of the base metal hardness value at a distance of 13 mm (480 HV) from the weld metal center. The higher hardness values could be attributed to the existence of martensitic structure in this region as a result of higher cooling rate.

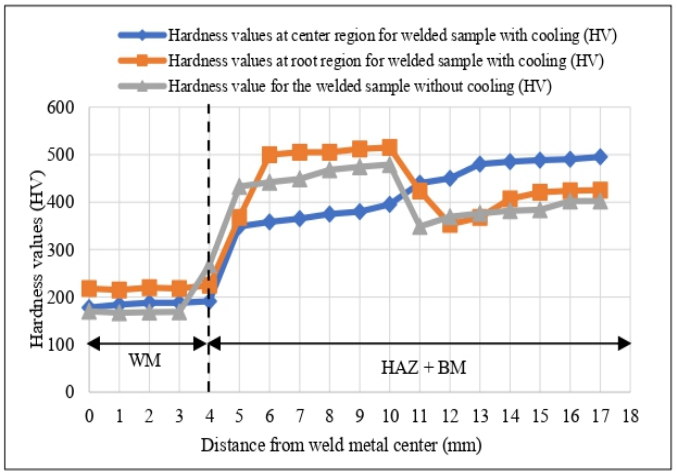

Fig -17: Hardness distribution in the specimen welded using AWS A5.18 ER 70S-6 / MAG and applying single bevel joint.

Figure. 18 shows the hardness distribution of the joint welded using AWS A5.9 ER 307 filler wire and applying a single V groove joint. Hardness increases from weld metal to a high value at the HAZ. Retainment of the base metal hardness occurred at a distance of 14 mm from the weld metal center (450 HV) with the application of cooling. However, the retainment of base metal hardness does not occur at a distance of 16 mm without cooling application

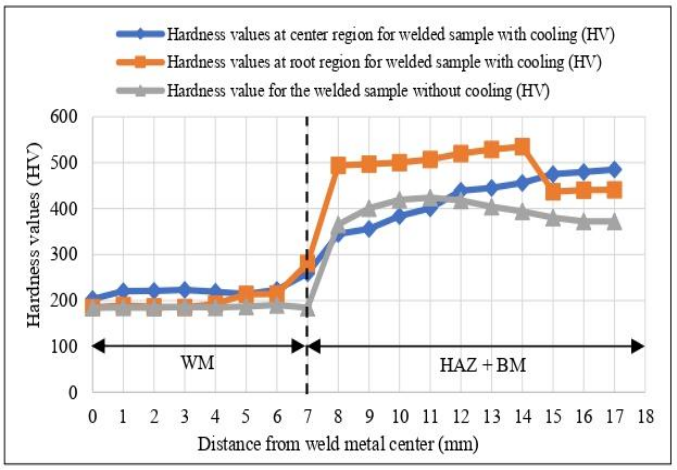

Fig -18: Hardness distribution in the specimen welded using AWS A5.9 ER 307/ MIG and applying single V joint.

Figure. 19 shows the hardness distribution of the joint welded using AWS A5.9 ER 307 filler wire and applying a single bevel groove joint. Hardness kept increasing gradually with a retainment of the base metal hardness value at a distance of 13 mm (450 HV) from the weld metal center.

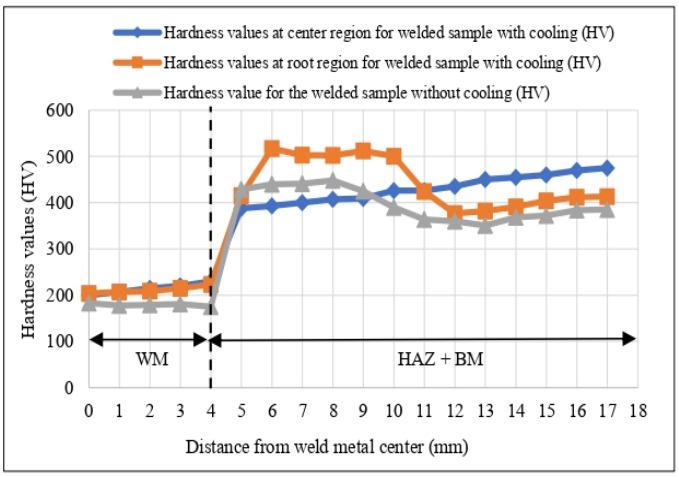

Fig -19: Hardness distribution in the specimen welded using AWS A5.9 ER 307/ MIG and applying single bevel joint.

3.7. Effect of dilution on weld metal properties

Figure 20 shows the dilutions percentage of the single V and bevel groove joints with the GMAW welding process using AWS A5.18 ER70S-6 and AWS A5.9 ER 307 filler wires. The dilution in the single V joint was less than the single bevel joint using AWS A5.18 ER70S-6 filler wire. The dilution process affects greatly the mechanical and metallurgical properties of weld metal that deviate from the pure filler wire properties. This can be observed in the tensile strength of welded joint as shown in Table. 8 as mentioned in section 3.8. Also, the dilution affects the microstructure of weld metal as shown in Fig.15. b (see section 3.5). The existence of martensite structure greatly affects the improvement of tensile strength.

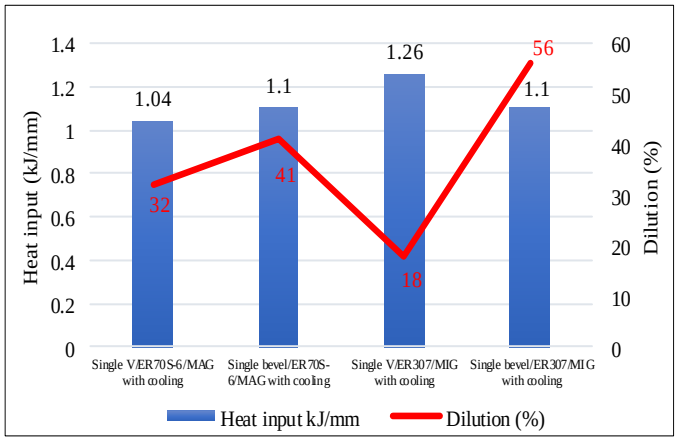

Fig -20: Effect of joint types, heat input, and filler metals on dilution.

Figure 21 shows the Schaeffler diagram indicating two different dilution levels using a single V groove (18 % dilution) and single bevel groove (56 % dilution) when applying AWS, A 5.9 ER 307 as a filler metal. The Figure indicating that the microstructure of the weld metal is mainly austenite and delta ferrite using single V (18 % dilution). On the other hand, the microstructure of the weld metal is mainly martensite and austenite using single bevel groove (56 % dilution). This was confirmed with the observation of microstructures shown in Fig. 14 and 15.

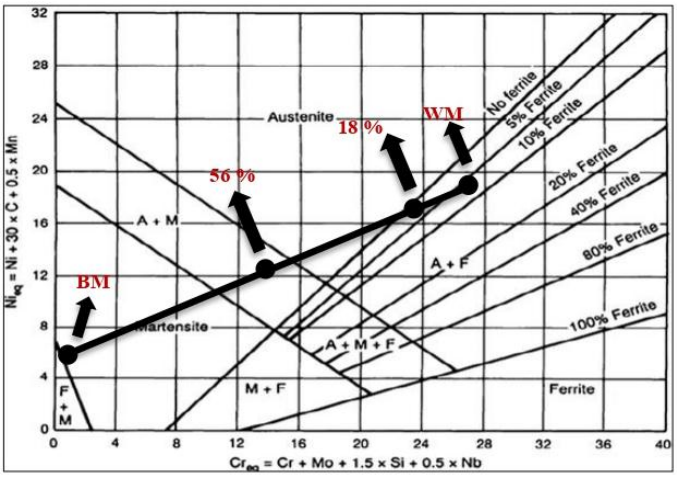

Fig -21: Schaeffler diagram indicating the locations of pure weld metal (WM) base metal (BM) and the compositions of weld metal with different joints (different dilutions).

3.8. Tensile strength properties of welded joints

Table 8 and Fig. 22 show the ultimate tensile strength of welded joints using carbon steel and austenitic stainless-steel filler metals using single V and single bevel groove joints. In this Table, theoretical values of tensile strength for all filler metals (pure) used have been included [13]. From the data in Table 8 and Fig.22, it was found that in all cases the requirements for qualification are fulfilled. An increase in ultimate tensile strength of welded metal with respect to the filler metal was also found. This could be as a consequence of an increase in dilution percentage. The fractures are located in the weld metal in all specimens whether using carbon steel and austenitic stainless-steel filler wires.

3.9. Impact energy properties of welded joints

Table 9 and Fig.23 show the Charpy V notch impact tests results of tests conducted at room temperature and at - 40 ºC in the weld metal region. In addition, the Charpy V notch impact test was conducted at room temperature and at - 40 ºC in the heat-affected zone region. An increase in impact energy joint welded using AWS A 5.9 ER 307 filler metal shows a significant increase in impact resistances shown in Fig. 23 and Table 9. All weld metal notched impact specimens were fractured at weld metals. However, all HAZ notched impact specimens were fractured at HAZ.

Table -8: Tensile strength properties of welded joints

Joint type and filler metal classification	Tensile strength of samples without cooling, MPa	Tensile strength of samples with cooling, MPa	Fracture location	Strength of all weld metal (pure) used, MPa, [6, 20]
Single V/ AWS A 5.18ER70S-6	719.92	845.5	WM	540
Single bevel/ AWS A 5.18 ER70S-6	815.03	890.5	WM	540
Single V/ AWS A 5.9 ER 307	824.31	867.14	WM	620
Single bevel / AWS A 5.9 ER 307	834	898.5	WM	620

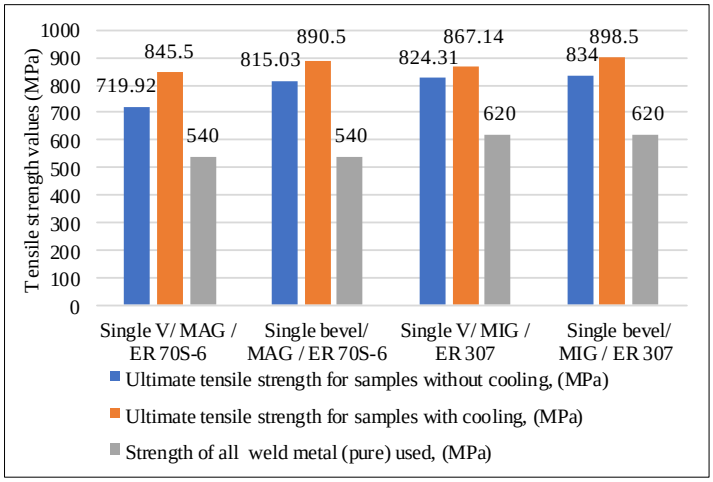

Fig -22: Tensile strength properties values of welded joints

Table -9: Impact energy properties values of welded joints

Joint type and filler metal classification	Charpy V notch (CVN) results in (J)							
	WM at RT, without cooling	WM at - 40°C, without cooling	WM at RT, with cooling	WM at - 40°C, with cooling	HAZ at RT, with cooling	HAZ at - 40°C, with cooling	CVN of the used filler metal at RT, [20]	CVN of the used filler metal at - 40°C, [20]
Single V/AWS A 5.18 ER70S-6	105	41	132	61	90	78	120	50
Single bevel /AWS A5.18 ER70S-6	75	32	84	51	85	73	120	50
Single V/AWS A 5.9 ER307	85	51	95	63	140	130	120	110
Single bevel/AWS A 5.9 ER307	43	61	134	65	133	126	120	110

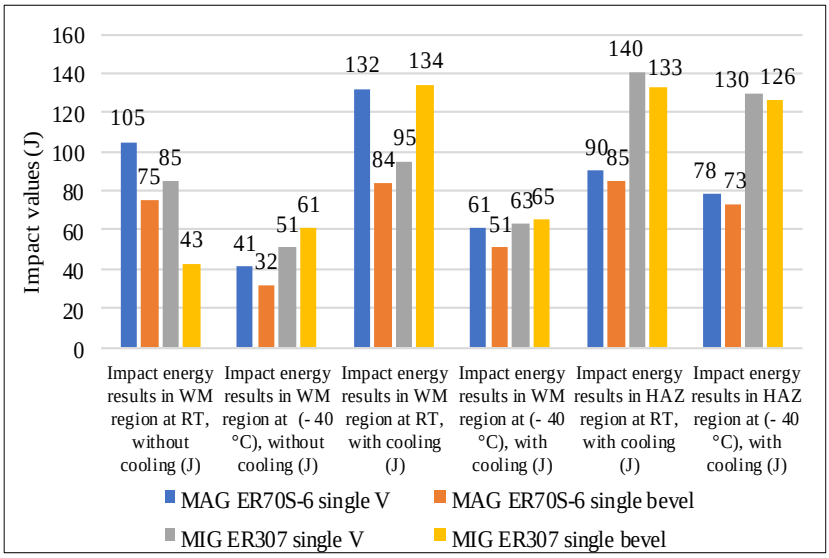

Fig -23: Impact test values of welded joints

3.10. Corrosion behaviour of welded joints

Table 10 and Figure 24 show the potentiodynamic polarization curves as well as the corrosion parameters of the base metal and the welding regions. The base metals have a tempered martensite microstructure. The GMAW process used welding filler wires of either carbon steel AWS A5.18 ER70S-6 with ferrite-pearlite microstructure or austenitic stainless steel with austenite columnar structure microstructure. The GMAW process applied both single V and single bevel groove joints. Results show that the corrosion rates of welded joints are lower than the base metal. It is worthy to mention that the single bevel welded joints give much lower corrosion rates than the base metal and the single bevel welded joints performed using austenitic stainless-steel filler wire compared to single bevel welded joint performed using carbon steel filler wire. Potentiodynamic polarization curves indicate the shift of Ecorr in the noble (positive) direction in the case of welded joints performed using austenitic stainless-steel filler wire. However, the noble shift of Ecorr is much higher in the case of a single bevel welded joint. It is also noticed that the positive shift of Ecorr is accompanied by a reduction in the measured anodic current.

Table -10: Comparison between corrosion parameters of the base metal region and all welded joints

Samples	E_{corr} (V)	I_{corr} (A/Cm^2)	Corrosion rate mm/year
Base metal	-0.598	$7.97x10^{-6}$	0.0598
Single V/AWSA5.18 ER70S-6 with cooling	-0.640	$6.73 x10^{-6}$	0.0515
Single bevel/AWSA5.18 ER70S-6 with cooling	-0.646	$2.00 x10^{-6}$	0.0150
Single V/AWSA5.9 ER307 with cooling	-0.571	$6.66 x10^{-6}$	0.0495
Single bevel/AWSA5.9 ER307 with cooling	-0.316	$1.32 x10^{-6}$	0.0127

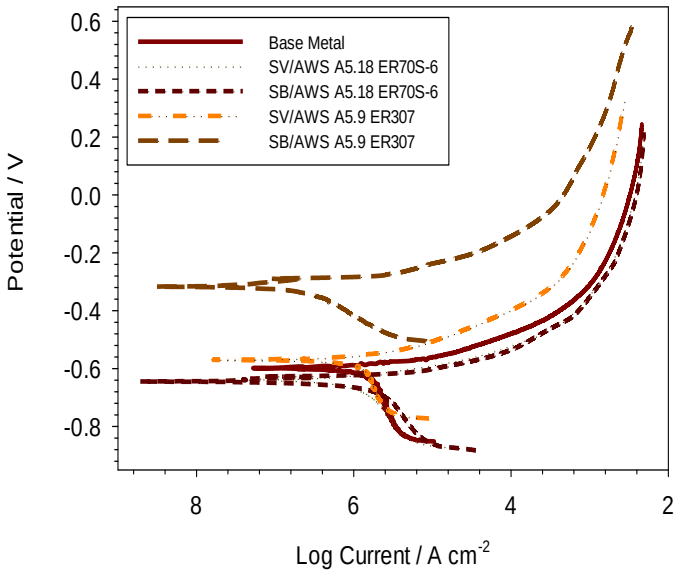

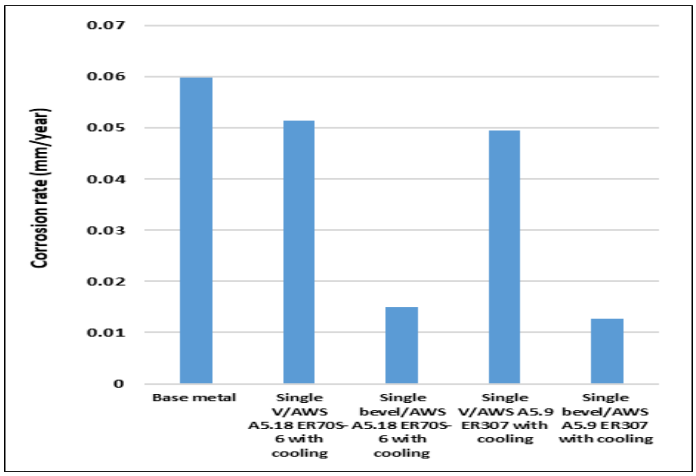

Fig -24: Comparison between corrosion rate of base metal and all welded joints.

3.10.1. Microstructure of corrosion behaviour of welded joints

The reduced corrosion resistance of the base metal compared to the welding joints may be attributed to its tempered martensite microstructure with a lath shape morphology and a high density of dislocations [30]. On the other hand, the ferrite-pearlite microstructure of the welding joints performed using carbon steel filler wire makes it less susceptible towards corrosion attack. The austenitic microstructure of the welding joints performed using stainless steel filler wire makes it the highest corrosion resistance amongst the tested materials. The enhancement of the corrosion resistance of the austenitic stainless is attributed to its high content of Cr, and Ni resulting in the formation of a passive film that protects the metal from corrosion [31]. The presence of Mo in the austenitic stainless further improves its corrosion resistance by the improvement of the passive film quality and treats defects and imperfections that may exist in the film [30, 31].

4. CONCLUSIONS

The designed welding procedure using the GMAW with AWS A 5.18 ER70S-6 and AWS A 5.9 ER307 filler metal were found to be a suitable option for welding armor steel, based on the results obtained in mechanical and metallurgical observation of welded joints. The following results can be concluded.

1. In MAG welding process using AWS A5.18 ER70S-6 filler wire, both single V and single bevel joints passed the required tensile strength by the military standard. Moreover, with MIG welding process using AWS A5.9 ER307 filler wire, both joints passed the required tensile strength by the military standard.

2. Dilution was observed in single V welded joints using both carbon steel and austenitic stainless-steel filler metal. The dilution percentage increased in single bevel welded joints using both carbon steel and austenitic stainless steel.

3. The ultimate tensile strength of welded joints using a single bevel is slightly higher than that of joints welded using a single V-groove. This could be attributed to the increase in dilution percentage with the single bevel joints.

4. An increase in cooling rate is accomplished by applying a compressed air (6 bar) cooling immediately after completion of each pass until the temperature falls to 100 °C. Also, a reduction in heat input was performed by a decrease in welding current. This resulted in a significant increase in joint strength and retainment of base metal hardness value at a shorter distance from the centreline of weld metal (lower than 14 mm).

5. A softening region at the HAZ is formed due to the over-tempering of the martensitic structure with a reduction in hardness values. This softening zone is much reduced in width with the increase in its hardness values with the application of cooling and reduction of heat input.

6. Both single V-joint and single bevel joint passed the required absorbed energy in Charpy V notch impact at - 40 °C tests whether using carbon steel and austenitic stainless-steel filler wire.

7. Results show that the corrosion rates of welded joints are lower than the base metal. It is worthy to mention that the single bevel welded joints give much lower corrosion rates than the base metal and the single bevel welded joints performed using austenitic stainless-steel filler wire compared to single bevel welded joint performed using carbon steel filler wire. Potentiodynamic polarization curves indicate the shift of Ecorr in the noble (positive) direction in the case of welded joints performed using austenitic stainless-steel filler wire. However, the noble shift of Ecorr is much higher in the case of a single bevel welded joint. It is also noticed that the positive shift of Ecorr is accompanied by a reduction in the measured anodic current.

NOMENCLATURE

CVN	Charpy V Notch Impact Test
Δt 8/5	The Difference in Temperature Between 800 °C to 500 °C
Δt 6/2	The Difference in Temperature Between 600 °C to 200 °C

REFERENCES

[1] Scazzosi, R.; Giglio, M.; Manes, A. (2021), "Experimental and Numerical Investigation on the Perforation Resistance of Double-Layered Metal Shields Under High-Velocity Impact of Soft-Core Projectiles", Eng. Struct., 228, 111467.

[2] Lazić Vukić, Arsić Dušan, Nikolić Ružica, Uhričik Milan, Hadzima, Branislav. (2019), "Influence of the Welding Joint type on Safety Properties of the Armor Steel ARMOX 500T", Materials Science. System Safety: Human - Technical Facility – Environment. volume 1, issue 1, pp. 753-759.

[3] Igor Barényi, Jozef Majerík, Ján Bezecný, Michal Krbaťa, Josef Sedlák, Aleš Jaroš. (2019), "Material and Technological Aspects while Processing of Selected Ultra High Strength Steel", Manufacturing Technology, ISSN 1213–2489, Vol. 19, No. 2 PP184-189.

[4] Balakrishnan M., Balasubramanian V., Reddy G. M. (2013), "TEMP Effect of Hard-Faced Interlayer Thickness on Ballistic Performance of Armour Steel Welds", Materials and Design, 44 (2013) 59–68.

[5] Lazić, V., Arsić, D., Nikolić, R. R., Djordjević, D., Prokić-Cvetković, R., Popović, O. (2017), "Application of the High Strength Steel HARDOX 450 for Manufacturing of Assemblies in the Military Industry", Key Engineering Materials, 755, 96-105.

[6] Morsy Amin Morsy, Rashad El Hebeary. (2019), 'Weldability of Armor Steel'', 72nd IIW Annual Assembly and International conference, 7-12 July 2019, PP 2-10.

[7] Arkadiusz Popławski, Piotr Kędzierski, Andrzej Morka. (2020), "Identification of Armox 500T Steel Failure Properties in the Modelling of Perforation Problems", Materials & Design, ELSEVIER, Volume 190, May 2020, 108536.

[8] Ivica Garašić, Maja Jurica, Dario Iljkić, Ante Barišić. (2019), "Determination of Ballistic Properties on ARMOX 500T Steel Welded Joint", Engineering Review, Vol. 39, Issue 2, 186-196.

[9] Saiprasad. P.V, Surendra. I.V, Narayan. K. L, Narasimha Rao. L.N.V. (2014), "Evaluation of Percentage of Dilution in Gas Metal ARC Welding", ISSN: 2249-5762, IJRMET Vol. 4, PP 131-134.

[10] Grujicic. M, Ramaswami. S, Snipes. J.S, Yavari. R, Yen. C.F, Cheeseman B.A. (2015), "Optimization of Gas Metal Arc Welding GMAW Process for Maximum Ballistic Limit in MIL A46100 Steel Welded All-Metal Armor", Journal of Materials Engineering and Performance volume 24, pages229–244 (2015).

[11] Arsić, D., Nikolić, R., Lazić, V., Hadzima, B., Aleksandrović, S., Djordjević, M. (2014), "Weldability Estimates of Some High Strength Steels", 42. International Conference "Zvaranie 2014", Tatranská Lomnica, Slovakia, 11-21.

[12] Tekin Özdemir. (2020), "Mechanical & Microstructural Analysis of Armor Steel Welded Joints", International Journal of Engineering Research and Development, UMAGD 12, 166-175.

[13] Robledo D.M, Gomez J.A.S, Barrada J.E.G. (2011), "Development of a Welding Procedure for MIL A 46100 Armor Steel Joints Using Gas Metal Arc Welding", 78, 168,65-71.

[14] SSAB OXELOSUND SWEDEN: The steel book. Sweden, 2008. [online 10.6.2012]. Available: http://www.ssab.com.

[15] Magudeeswarana V.G, Balasubramanianb G, Madhusudan Reddy. (2018) Metallurgical characteristics of armour steel welded joints used for combat vehicle

construction. Defense Technology Volume 14, Issue 5, Pages 590-606.

[16] Ambuj Saxena, Shashi Prakash Dwivedi, Shubham Sharma, Vishal Shankar Srivastava. (2021) A comparative numerical analysis on the effect of welding consumables on the ballistic resistance of SMAW joints of armor steel. Appl. Sci. 2021, 11, 3629.

[17] Krishna Murthy. N, Janaki Ram. G. D, Murty. B. S, Reddy. G. M, Rao. T. J. P. (2014) Carbide-free bainitic weld metal: A new concept in welding of armor steels. Metallurgical and Materials Transactions B volume 45, pages2327–2337.

[18] SSAB Armox welding recommendations., SSAB OxelOsund AB: OxelOsund, Sweden (2005).

[19] Voestalpine (2019) Böhler of welding product catalogue. P30 - P360.

[20] ESAB. (2016) Welding filler metal, DATABOOK, 2016.

[21] Do DEFENSE, MIL STD 1185. (1979) Military Standard. Welding, high hardness armor, DoD, DEPARTMENT OF DEFENSE.

[22] Arkadiusz Popławski, Piotr Kędzierski, Andrzej Morka. (2020) Identification of armox 500T steel failure properties in the modelling of perforation problems. Materials & Design, ELSEVIER, Volume 190, May 2020, 108536.

[23] DAVID MAZUERA ROBLEDO, JOHN ALBERTO SUÁREZ GÓMEZ, JORGE ENRIQUE GIRALDO BARRADA. (2011) Development of A welding procedure for MIL A 46100 armor steel joints using gas metal arc welding. Dyna, año 78, Nro. 168, pp. 65-71. Medellín, Agosto.

[24] Purvesh K Nanavati. (2020), "Importance of Dilution in Dissimilar Metal Welding and Calculations of Weld Metal Compositions", Welding Knowledge.

[25] American Society for Testing and Materials. Standard Test Method for Knoop and Vickers Hardness of Materials, ASTM E384-11. 2011.

[26] American Society for Testing and Materials. Standard Test Methods and Definitions for Mechanical Testing of Steel Products, ASTM A370-14. 2014.

[27] American Society for Testing and Materials. Standard Test Methods for Notched Bar Impact Testing of Metallic Materials, ASTM, E23-1a. 2002.

[28] Peng Liu, Shanguo Han, Yaoyong Yi, Cuixia Yan (2018), "Corrosion Behavior of Welded Joint of Q690 wif CMT Twin", International Journal of Corrosion, vol. 2018, Article ID 2368717, 9 pages.

[29] Aleksandar Cabrillo, Katarina Geric. (2016), "Weldability of high hardness armor steel", Advanced Materials Research 1138, 79-84.

[30] Dazheng Zhang, Xiuhua Gao, Guanqiao Su, Zhenguang Liu, Ningning Yang, Linxiu Du, and R.D. Misra (2018). "Effect of Tempered Martensite and Ferrite/Bainite on Corrosion Behavior of Low Alloy Steel Used for Flexible Pipe Exposed to High-Temperature Brine Environment", ASM International, JMEPEG 27:4911–4920.

[31] Chuaiphan Wichan, Srijaroenpramong Loeshpahn (2012). "Effect of Filler Alloy on Microstructure, Mechanical and Corrosion Behavior of Dissimilar Weldment between Aisi 201 Stainless Steel and Low Carbon Steel Sheets Produced by a Gas Tungsten Arc Welding", Advanced Materials Research 581-582(1):808-816.

BIOGRAPHIES

M. A. Morsy is a professor of welding technology at CMRDI, Cairo, Egypt. He is currently the head of the welding and NDT department in CMRDI, Cairo, Egypt. His Ph.D. in welding and production engineering from OSAKA University Japan. He publishes more than 50 papers in metal science, failure analysis, and welding technology.

Sabry. M. Abdel Aziz is a Ph.D. Researcher in the production technology department faculty of technology and industrial education, Helwan University, Cairo, Egypt. He obtained M.Sc. (2018) in production technology (material technology specialty). from Helwan University in Cairo.

Khaled Abdelwahed is an assistant professor of the automotive and tractors technology department, faculty of technology and industrial education, Helwan University, Cairo, Egypt. His Ph.D. in automotive technology from Helwan University, Cairo, Egypt. His research interest includes automotive, and tractors engineering.

Sabreen A. Abdelwahab is an associate Professor at Production Technology Department, Helwan University. She received her Ph.D. (2015) in Mechanical Engineering, Faculty of Engineering at Ain Shams University, Cairo-Egypt. Her research interest includes mechanical engineering, mechatronics, robotics, and automatic control.